ARTICLE

https://doi.org/10.1038/s41586-018-0843-2

Timing of archaic hominin occupation of Denisova Cave in southern Siberia

Zenobia Jacobs[1,2,8]*, Bo Li[1,2,8], Michael V. Shunkov[3,4], Maxim B. Kozlikin[3,5], Nataliya S. Bolikhovskaya[3,6], Alexander K. Agadjanian[3,7], Vladimir A. Uliyanov[3,6], Sergei K. Vasiliev[3,4], Kieran O'Gorman[1], Anatoly P. Derevianko[3,5] & Richard G. Roberts[1,2]*

The Altai region of Siberia was inhabited for parts of the Pleistocene by at least two groups of archaic hominins—Denisovans and Neanderthals. Denisova Cave, uniquely, contains stratified deposits that preserve skeletal and genetic evidence of both hominins, artefacts made from stone and other materials, and a range of animal and plant remains. The previous site chronology is based largely on radiocarbon ages for fragments of bone and charcoal that are up to 50,000 years old; older ages of equivocal reliability have been estimated from thermoluminescence and palaeomagnetic analyses of sediments, and genetic analyses of hominin DNA. Here we describe the stratigraphic sequences in Denisova Cave, establish a chronology for the Pleistocene deposits and associated remains from optical dating of the cave sediments, and reconstruct the environmental context of hominin occupation of the site from around 300,000 to 20,000 years ago.

The period of existence and geographical distribution of Neanderthals and their sister group, the Denisovans[1,2], are key unresolved issues in the study of human evolution and dispersal. Denisovan remains are known only from the type locality of Denisova Cave, which is located in the foothills of the Altai Mountains in southern Siberia (51° 23′ 51.3″ N, 84° 40′ 34.3″ E; Fig. 1a). Neanderthal remains have also been recovered from the deposits of this cave.

The cave consists chiefly of three large chambers—named Main Chamber, East Chamber and South Chamber (Fig. 1b)—each containing several metres of deposit. The stratified sequences are numbered by layer; layers with the same number in the different chambers are not necessarily equivalent in age[2]. Excavations have yielded Middle Palaeolithic stone artefacts and a variety of Upper Palaeolithic artefacts, as well as the remains of fauna and flora[3–7]. The fragmentary remains of four Denisovans, two Neanderthals and a daughter of Neanderthal and Denisovan parents have also been recovered[8–10]; their genomes have been sequenced[1,2,11–16], as has DNA extracted from the Pleistocene sediments[17].

The time of deposition of the youngest Pleistocene layers in the cave is currently constrained by radiocarbon (^{14}C) ages for charcoal fragments and bone collagen. However, many of these ages approach or exceed the limit of ^{14}C dating (about 50 thousand years ago (ka)) and the large spread in ages is consistent with field observations of post-depositional disturbance in some parts of the site (for example, layers 11.1 and 11.2 in East Chamber)[2]. Using a light-sensitive thermoluminescence signal[18], seven dates have been reported for quartz grains extracted from the deeper deposits in Main Chamber[3,19], ranging from 282 ± 56 ka (lower part of layer 22.2) to 69 ± 17 ka (layer 14.1). Although questions remain about some of the methodological aspects[20], these dates broadly agree with biostratigraphic data for the cave deposits[3]. Geomagnetic excursions recorded in layers 22.1 and 22.2 (Main Chamber)[21] were attributed to two events that are no longer supported[22,23]. DNA-based methods have been used to infer the ages of the hominin remains[11–13,16,24]. The oldest and youngest genetically dated Denisovan fossils—Denisova 2 (layer 22.1, Main Chamber) and Denisova 3 (layer 11.2, East Chamber), respectively—appear to differ in age by 54,200–99,400 years[13], with Denisova 3 tentatively dated to 85 ± 8 ka (95.4% confidence interval)[16,24]. DNA-based ages have also been estimated for the so-called Altai Neanderthal (Denisova 5, 123 ± 7 ka)[24] and the Neanderthal–Denisovan offspring (Denisova 11, dated to about 90 ka or later)[16], the latter of which has been dated by ^{14}C to more than 50 ka[15]. Further details are given in the Supplementary Information.

Collectively, these dates suggest that hominins have inhabited Denisova Cave intermittently since the middle of the Middle Pleistocene. However, accurate and more precise chronologies and a higher density of ages are required to address issues of site formation, hominin occupation and environmental conditions in the vicinity of the cave. Here we present details of the stratigraphy and report more than 100 new ages for the Pleistocene sequences in all three chambers, using optical dating of sediments[25–28] to construct a common timeline for the cultural remains, hominin fossils and palaeoecological records.

Stratigraphy and site formation

Denisova Cave is formed in Silurian limestone and covers a total area of about 270 m^2. Main Chamber is about 10 m high and contains approximately 6 m of deposits, which were first excavated 40 years ago. East Chamber and South Chamber are both narrow (less than 3 m wide) and extend away from Main Chamber (Fig. 1b and Extended Data Fig. 1a); their deposits have been excavated to depths of about 7 and 4.5 m, respectively. The upper 1.5–2 m of deposit in each chamber (layers 0–8) are Holocene in age. The underlying Pleistocene deposits consist of clay, silt and sand grains (that were blown or washed into the cave, or were reworked from pre-existing cave sediments) interstratified with coarser, angular limestone debris (gravel-size and larger) spalled from the floor, walls and roof of the cave owing to physical and chemical weathering of the bedrock.

The Pleistocene sequences (Fig. 2) are complex and include laterally discontinuous layers and unconformities between layers (due to erosional events or depositional gaps), as well as evidence of post-depositional modifications due to chemical diagenesis and freeze–thaw processes, subsidence and slumping, animal burrowing,

[1]Centre for Archaeological Science, School of Earth, Atmospheric and Life Sciences, University of Wollongong, Wollongong, New South Wales, Australia. [2]Australian Research Council (ARC) Centre of Excellence for Australian Biodiversity and Heritage, University of Wollongong, Wollongong, New South Wales, Australia. [3]Institute of Archaeology and Ethnography, Russian Academy of Sciences, Siberian Branch, Novosibirsk, Russia. [4]Novosibirsk State University, Novosibirsk, Russia. [5]Altai State University, Barnaul, Russia. [6]Lomonosov Moscow State University, Moscow, Russia. [7]Borissiak Paleontological Institute, Russian Academy of Sciences, Moscow, Russia. [8]These authors contributed equally: Zenobia Jacobs, Bo Li. *e-mail: zenobia@uow.edu.au; rgrob@uow.edu.au

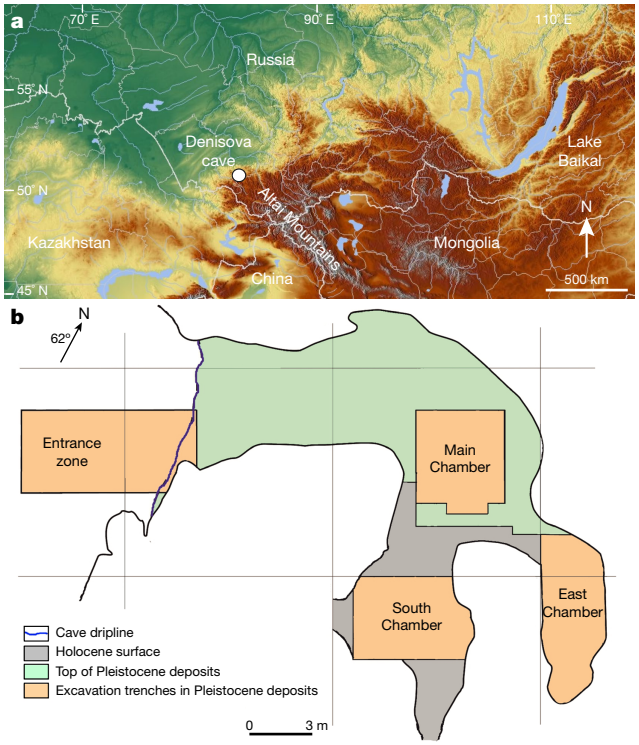

Fig. 1 | Location of Denisova Cave and site plan. a, Map of southern Siberia and site location. **b**, Plan of cave interior showing Main Chamber, East Chamber and South Chamber; the entrance zone was not investigated in this study.

and anthropogenic activities (Supplementary Tables 16–18). The layers cannot be traced stratigraphically between the chambers, but field observations of sedimentary characteristics and morphological features permit correlation of some Pleistocene layers (for example, 22).

The Pleistocene deposits in Main Chamber comprise layers 9–22 and their subdivisions (Fig. 2a and Extended Data Figs. 2, 5a, b). Most of the layers are composed of a poorly sorted, sandy-silt matrix with abundant angular clasts of spalled bedrock. Some layers (for example, 9 and 21) have fewer coarse clasts. Many of the layer boundaries are indistinct and transitional. Layer 22.1 forms a peak-shaped feature in the south-east profile and incorporates many vertically tilted gravel clasts. The two overlying layers (21 and 20) follow the same topography. There is no evidence for substantial mixing of sediments between these three layers. Layer 12 marks the start of the sub-horizontal stratigraphy in this chamber. Parts of some layers show signs of animal burrowing (for example, 9 and 13), freeze–thaw processes (for example, 11 and 22.1), phosphatization (layer 9 in particular), manganese staining and other diagenetic alterations.

In East Chamber, the basal 2 m of deposit (layer 17.2) consists mainly of fine-grained sediments (silty clay) deposited in a former phreatic tube (Fig. 2b and Extended Data Figs. 3, 5c–e). The overlying layer (17.1) has a similar composition and is, in turn, overlain by a thin band of organic-rich sediment (layer 16); both layers follow the undulating topography of the narrow bedrock shelf that separates the phreatic tube from the chamber above. The remaining Pleistocene sequence (layers 15 to 9) is characterized by poorly sorted sediments composed of sandy silts with occasional-to-abundant angular clasts of limestone. Layers 17.1 to 11.1 dip inwards from the walls and sag towards the base of the chamber owing to post-depositional subsidence and possibly some slumping; carnivore coprolites (from cave hyenas) are common in these layers. Parts of layers 11 and 9 are heavily phosphatized[29] and show signs of disturbance (lack of bedding), especially from animal burrowing activities. Sediment mixing may also have occurred close to the chamber walls, where fissures are evident and the stratigraphy is complex.

Excavations in South Chamber are currently limited to the entrance area, where layers 9–22 are tentatively recognized (Fig. 2c and Extended Data Fig. 4). The lowest excavated unit is provisionally identified as layer 22, on the basis of its similar colour and texture to layer 22 in Main Chamber and its unconformable contact with the overlying unit, tentatively identified as layer 20. The latter is overlain by layers 9–19, which consist of poorly sorted sediments (silty sand with scattered to abundant clasts of spalled bedrock), and are commonly separated by indistinct and transitional boundaries. Layer 9 contains few coarse clasts, but is extensively phosphatized and burrowed in places (Extended Data Fig. 4d).

Pleistocene chronologies

We constructed numerical chronologies for the Pleistocene sequences in all 3 chambers from optical dating[25–28] of 103 sediment samples collected over 4 excavation seasons; 92 samples were dated from measurements of more than 280,000 individual grains of quartz and potassium-rich feldspar (K-feldspar), and 11 samples were dated using multi-grain aliquots of K-feldspar. Optical ages were determined using four methods of equivalent dose (D_e) estimation (see Methods) and were used to develop a Bayesian model for the depositional chronology in each chamber, to connect their stratigraphic sequences and to provide a composite age and environmental framework for hominin occupation of the site (Figs. 3, 4). We also compared these ages with previously published ^{14}C ages[2,15] for nine animal bones, a fragment of charcoal and a piece of Neanderthal bone from layers 11 and 12; no Denisovan remains have been dated directly. Details of sediment sample locations and collection, preparation, measurement, and data-analysis procedures are given in the Supplementary Information, together with the measured and modelled ages and related data.

Fifty-five sediment samples have been dated from Main Chamber (Extended Data Figs. 2, 5a, b). The optical ages are mostly in stratigraphic order and show that the deposits have accumulated episodically since the middle of the Middle Pleistocene (Fig. 3 and Extended Data Fig. 6). Finite ages for the deeper deposits (layers 22–13) could be obtained only using the K-feldspar post-infrared infrared stimulated luminescence (pIRIR) signal, because the optically stimulated luminescence (OSL) signal of quartz was saturated. The wide spread in dates for layer 13 (175–102 ka at 95.4% probability; Supplementary Table 7) is consistent with disturbance by burrowing animals[3], so these ages were omitted from the Bayesian model. Layer 22 accumulated before 287 ± 41 ka, followed by deposition of layers 21 and 20 between 250 ± 44 ka and 170 ± 19 ka, and layers 19–14 between 151 ± 17 ka and 97 ± 11 ka (here and below, we give modelled age estimates and total uncertainties at 95.4% probability). Layer 12 was deposited between 70 ± 8 ka and 58 ± 6 ka, before the accumulation of layer 11 between 44 ± 5 ka and 38 ± 3 ka. The final Pleistocene deposits are represented by layer 9, which unconformably overlies layer 11 and has start and end dates of 36 ± 4 ka and 21 ± 8 ka, respectively. There is some uncertainty about layer assignments where the stratigraphic boundaries are indistinct and transitional, and the small-scale mixing of parts of some layers is indicated by scatter in the single-grain D_e distributions and optical ages.

Thirty-seven sediment samples have been dated from East Chamber (Extended Data Figs. 3, 5c–e). The deposits in layers 17–12 have a stratigraphically coherent chronology (Fig. 3 and Extended Data Fig. 7), limited age variation within any particular layer and D_e distributions that show minimal evidence for mixing, which we attribute to the lack of substantial post-depositional disturbance. Layer 17 accumulated before 284 ± 32 ka (saturation of the pIRIR signal prevented estimation of a finite age for the deepest sample), followed by the deposition of layers 16–12.2 between 259 ± 28 ka and 129 ± 11 ka. Layers 12.1 and 11.4–11.1 were deposited between 120 ± 11 ka and 38 ± 9 ka. None of the samples collected from layers 11.4 or 11.3 show evidence of mixing. Five out of ten samples from layers 11.2 and 11.1 also show good integrity and give date ranges of 63 ± 6 ka to 55 ± 6 ka and 49 ± 6 ka to 38 ± 9 ka, respectively. The other five samples—and those from

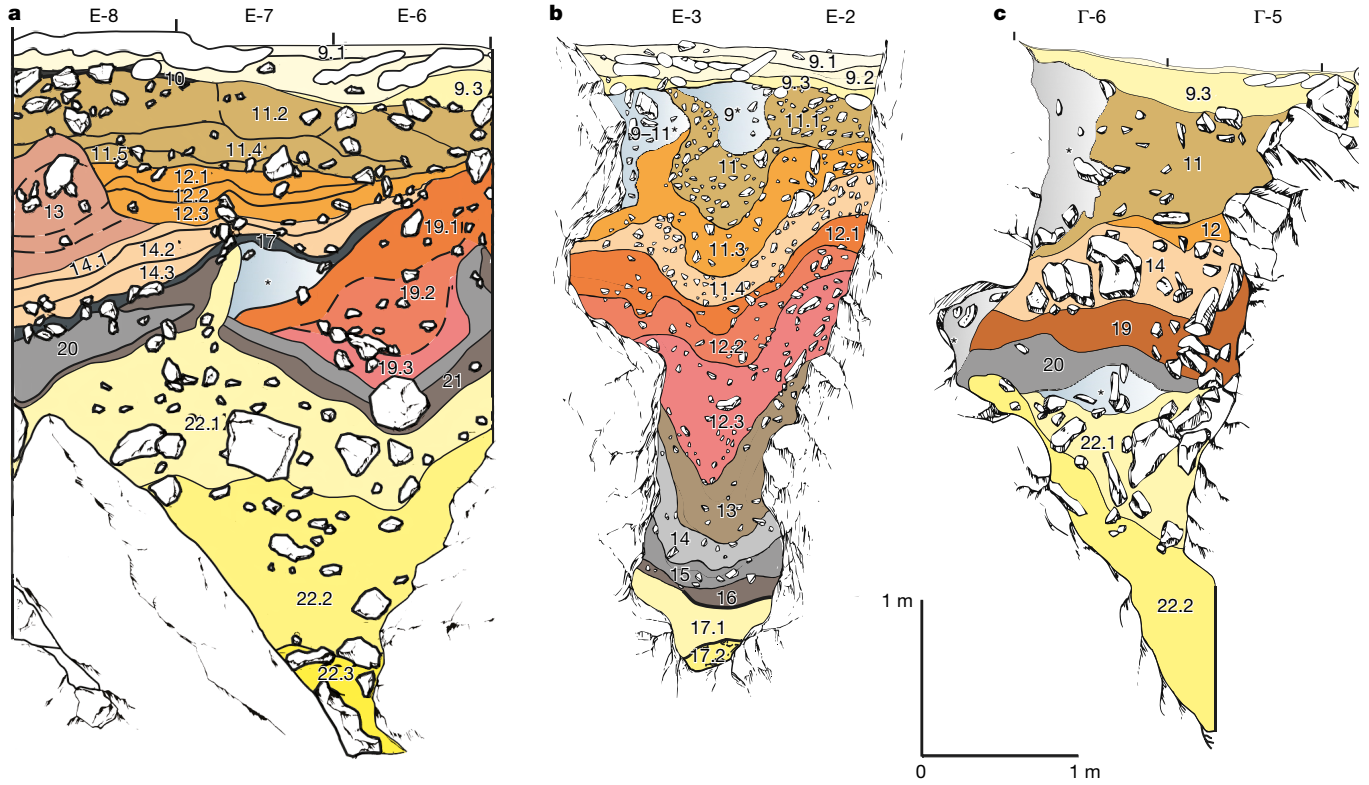

Fig. 2 | Stratigraphic sequences exposed in Denisova cave. a, Main Chamber. **b**, East Chamber. **c**, South Chamber. The southeast profile is shown for each chamber; these profiles were sampled for optical dating in 2012. Numbers denote stratigraphic layers, layer colours are notional and asterisks indicate areas of mixed deposit.

layers 9 and 8 in the southeast profile—have layer assignments that are uncertain or produced scattered D_e distributions from which reliable optical ages could not be determined (see Supplementary Information). We attribute these D_e distributions to disturbance of the deposit by hyenas and other burrowing animals, resulting in mixing of grains—and presumably also artefacts and fossils—of various ages, consistent with the wide spread in ^{14}C ages (from over 50,000 to about 19,000 calibrated years before present (BP; present is AD 1950) obtained for the upper part of layer 11 in this chamber[2].

Eleven sediment samples were dated from South Chamber (Extended Data Fig. 4). The lowest sampled unit (layer 22) accumulated before 269 ± 97 ka, followed by a lengthy time gap before deposition of layers 19 and 14 between 136 ± 26 ka and 101 ± 19 ka (Fig. 3 and Extended Data Fig. 8a). Layer 12 was deposited between 64 ± 9 ka and 47 ± 8 ka, consistent with ^{14}C ages of about 52,000 and over 50,000 calibrated years BP for bones from layer 11.2 (ref. [2]).

We also compared the OSL and pIRIR ages for 47 samples dated using both quartz and K-feldspar grains as an internal test of consistency (Extended Data Fig. 8b). The mean age-ratio is 1.00 ± 0.01 (standard error of the mean) and the mean ratio for each chamber is also consistent with unity. This implies that the cave sediments were bleached sufficiently at deposition to reset both dating signals (at least over the time span of this comparison), as OSL traps are emptied more rapidly and completely than are pIRIR traps[30,31]. Collectively, the three chambers contain a near-complete sequence of Pleistocene deposits (with some noticeable gaps in sedimentation) and hominin occupation extending from about 300 to about 20 ka (Figs. 3, 4).

History of hominin occupation

The oldest hominin fossil from the cave is a Denisovan molar (Denisova 2) recovered in 1984 from the top of layer 22.1 in Main Chamber (328–246 ka); however, the exact provenance of this tooth cannot now be established definitively. Denisovan DNA was retrieved from the sediments of layer 15 in East Chamber (217–185 ka) and from hominin remains in East Chamber (Denisova 8, 132–93 ka, and Denisova 3, 69–48 ka) and South Chamber (Denisova 4, less than 47 ± 8 ka). Neanderthal DNA was retrieved from sediments that were deposited between 168 and 86 ka in Main Chamber (layers 19, 17 and 14) and between 205 and 172 ka in East Chamber (layer 14), and from hominin remains in East Chamber (Denisova 9, 150–118 ka, and Denisova 5, 132–93 ka); the age range for Denisova 9 applies also to Denisova 11. Figures 3 and 4 show the association between the hominin fossils, sedimentary DNA remains and stratigraphic layers in each chamber. The DNA-based ages[13,24] for Denisova 5 and Denisova 8 are consistent with the optical ages for the associated layers; however, the estimates for Denisova 3 and Denisova 4 are older than expected based on their stratigraphic positions, whereas the ages for Denisova 11 and Denisova 2 are younger than expected. The omission of uncertainties associated with population size, mutation rate and generation interval in the genetic estimates[16,24] may account for some of these discrepancies, as might the re-deposition of these isolated and fragmentary fossils.

Four main artefact phases have been identified for hominin occupation of Denisova Cave during the Pleistocene: the early Middle Palaeolithic, middle Middle Palaeolithic, Initial Upper Palaeolithic and Upper Palaeolithic (examples of each of these phases are shown in Extended Data Fig. 9). Figure 3 and Extended Data Table 1 show the association between the artefact phases and layers in each chamber, and Supplementary Table 1 lists the number of artefacts recovered from each layer in Main Chamber and East Chamber. Early Middle Palaeolithic stone tools have been recovered from sediments deposited in Main Chamber and South Chamber before 287 ± 41 ka and 269 ± 97 ka, respectively, with the further development of early Middle Palaeolithic assemblages up to 170 ± 19 ka and 187 ± 14 ka in Main Chamber and East Chamber, respectively. In general, early Middle Palaeolithic stone tools are characterized by discoidal and Kombewa

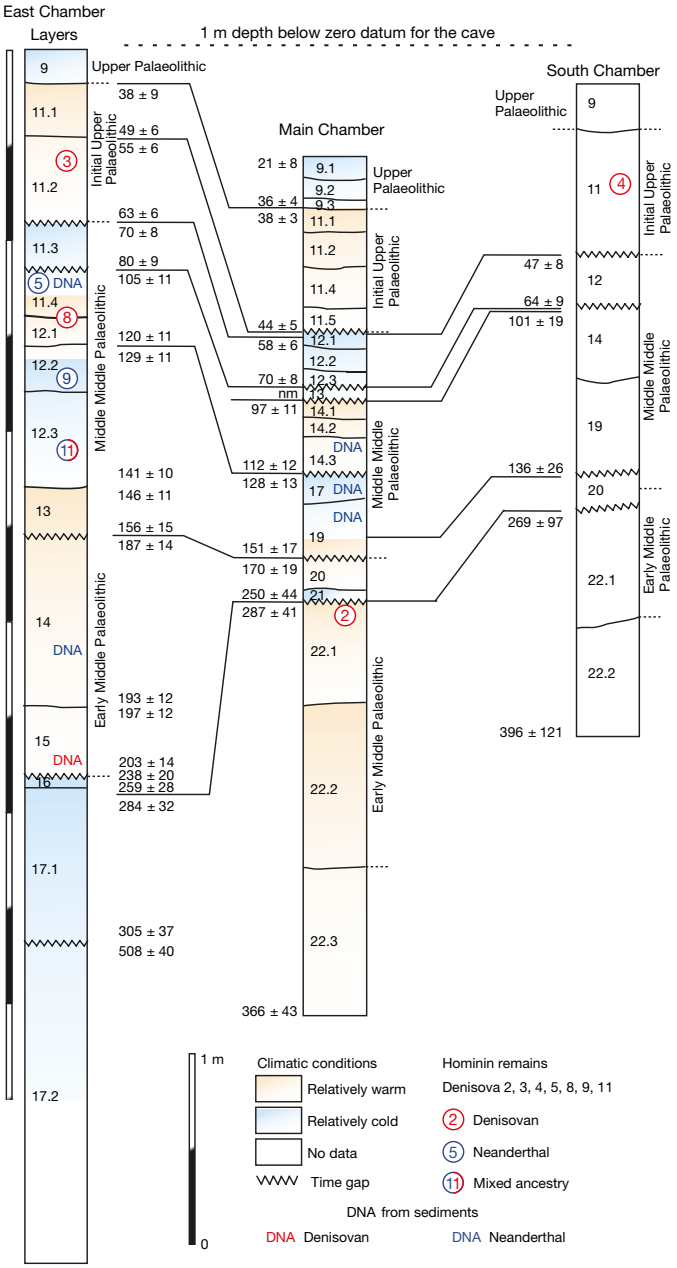

Fig. 3 | Chronological summary of hominin and environmental records in all three chambers. Layers containing skeletal remains and sedimentary DNA of Denisovans and Neanderthals are denoted by circled specimen numbers and by 'DNA', respectively (red, Denisovans; blue, Neanderthals; both colours, mixed ancestry). Artefact assemblages are indicated to the right of each stratigraphic sequence. Climatic conditions are inferred from pollen and faunal records (orange, relatively warm; blue, relatively cold; white, no data). Optical dates (in ka) are the Bayesian model estimates with total uncertainties at 95.4% probability; layer 13 in Main Chamber (labelled 'nm') was not included in the age model. Isochrons (lines of equal age) are used to correlate stratigraphic layers between chambers, and time gaps are indicated by wavy lines.

cores, the presence of Levallois cores for manufacturing flakes, and they include various types of scrapers, denticulates and notched tools (Extended Data Fig. 9d). The overlying middle Middle Palaeolithic layers were deposited between 156 ± 15 ka and 58 ± 6 ka in Main Chamber and East Chamber, and between 136 ± 26 ka and 47 ± 8 ka in South Chamber. In these assemblages, primary flaking is characterized by the use of flat, discoidal and Levallois cores; isolated sub-prismatic cores have also been identified. Scrapers dominate the tool assemblage, although notched-denticulate pieces are well represented, and end-scrapers, burins, chisel-like tools and truncated flakes are also present (Extended Data Fig. 9c).

The deposition of the Initial Upper Palaeolithic layers started before 44 ± 5 ka and 63 ± 6 ka in Main Chamber and East Chamber, respectively, and after 47 ± 8 ka in South Chamber; we note that the earliest artefacts were recovered from layer 11.2 in East Chamber, which has been disturbed in places. The Initial Upper Palaeolithic assemblages include variants of parallel and radial flaking, and narrow-faced cores for blade production and Levallois flaking (Extended Data Fig. 9b). Scrapers dominate the stone artefacts and various Upper Palaeolithic-type lithic implements represent a large proportion of the assemblage, which also yielded a rich collection of bone tools and ornaments made from animal teeth and bones, ivory and gemstones. The accumulation of Upper Palaeolithic assemblages (Extended Data Fig. 9a) started in Main Chamber at 36 ± 4 ka, with a well-developed stone bladelet technology and a Upper Palaeolithic component that is distinct from that of the Initial Upper Palaeolithic assemblages, and from the prevailing background of scrapers.

The archaeological, fossil hominin and sedimentary DNA evidence therefore currently suggests that the cave was occupied by Denisovans from 287 ± 41 ka (or, conservatively, from 203 ± 14 ka) to 55 ± 6 ka or later, if Denisova 3 and Denisova 4 are not intrusive. Neanderthals were also present at the site between 193 ± 12 ka and 97 ± 11 ka.

Environmental context

We have reconstructed the Pleistocene environments in the vicinity of Denisova Cave over the last approximately 350,000 years from the remains of animals and plants in Main Chamber and East Chamber[3–7] (Fig. 3 and Supplementary Information). Inferred conditions are relative to the current moderately continental climate (average January and July temperatures outside the cave of −16 °C and 18 °C, respectively). Reconstructions are based on analyses of the remains of 27 species of large mammals, more than 100 species of small vertebrates (40 species of small mammals, 66 taxa of birds and bones of fish, reptiles and amphibians) and pollen records for 30 species of tree, 36 shrub and grass taxa, and 6 species of spore-bearing plants.

The deposits that accumulated in late marine isotope stage (MIS) 9 did so under fairly warm and moderately humid conditions, characterized by forests dominated by pine and birch and a considerable admixture of broad-leaved species. The subsequent period of moderate cooling in early MIS 8 was marked by a reduction in forest cover, followed by an interval of relatively stable climate that was accompanied by the maximum spread of forest seen over the time span of our environmental reconstruction. Subsequent sedimentation in MIS 8 took place in a relatively cold and moderately humid climate, during which mountain tundra and forest–tundra landscapes developed in the vicinity of the cave. During MIS 7, and possibly early MIS 6, sediments were deposited under warm and relatively dry conditions, which were accompanied by the widespread emergence of pine–birch forests and broad-leaved species. Steppe and meadow–steppe communities flourished during the cold and dry periglacial conditions of terminal MIS 6.

Conditions were unstable during MIS 5, and incorporated environments that were variously drier, warmer, cooler and milder than the present-day environment. Climatic deterioration during MIS 4 was accompanied by multiple turnovers of plant associations under alternating dry and wet cold conditions; steppe and meadow–steppe communities expanded considerably, whereas birch, alder and broad-leaved species disappeared. During MIS 3, dark coniferous forests and meadow associations expanded when conditions were cool and humid, whereas mixed-grass communities and forest (including broad-leaved species) spread when conditions were warmer. In the millennia leading up to the last glacial maximum at about 20 ka, the climate fluctuated between moderately cold (dominated by spruce forests) and cold and dry (dominated by tundra–steppe associations).

There is broad agreement in the interpretation of climatic conditions between the three chambers—which can be linked using the chronological framework established in this study—and with global and other

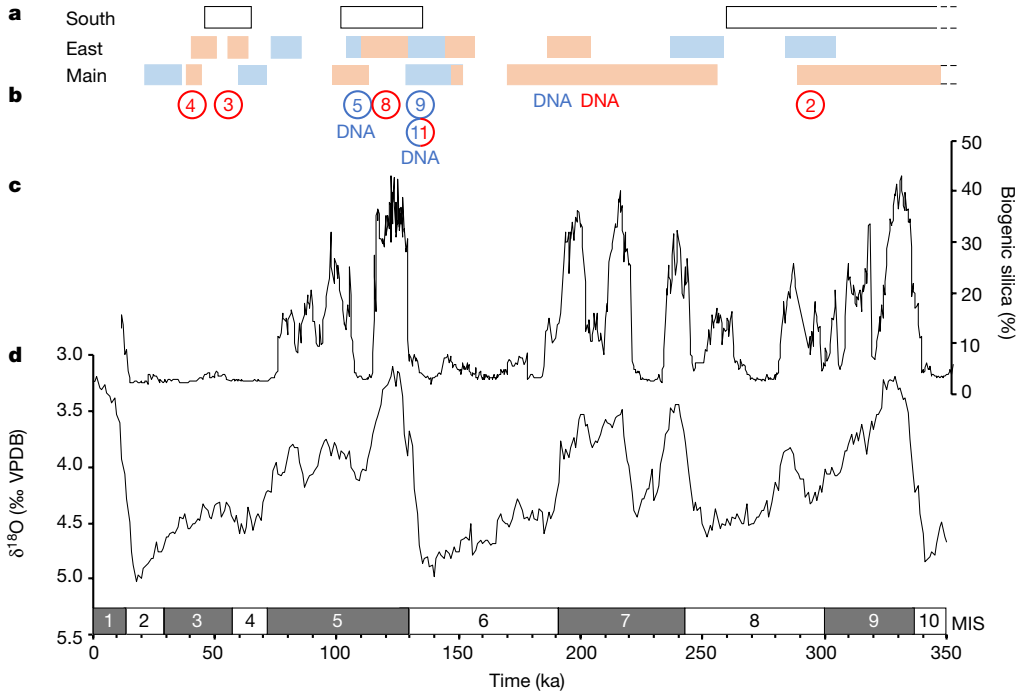

Fig. 4 | Comparison of environmental records at Denisova Cave with global and regional climate proxies. a, Climatic conditions inferred from pollen and faunal records in Main Chamber, East Chamber and South Chamber (orange, relatively warm; blue, relatively cold; white, no data) plotted on a calendar-year timescale; the time span of each climatic interval is demarcated by the mean start and end ages for the relevant layers (Fig. 3). Marine isotope stage (MIS) boundaries follow a previous publication[40]. **b**, Fossils (circled specimen numbers) and sedimentary DNA ('DNA') of Denisovans (red) and Neanderthals (blue) and a fossil of mixed ancestry (both colours). **c**, Composite BDP-96 biogenic silica record of diatom productivity in Lake Baikal[32], located about 1,600 km east of Denisova cave. **d**, LR04 stack of marine benthic foraminiferal isotopic ($\delta^{18}O$) data assembled from 57 globally distributed sites[40] (VPDB, Vienna Pee Dee Belemnite).

regional records[32–35] (Fig. 4). The largest anomaly between inferred climate and timing is at approximately 150 ka, at which time the pollen assemblages in East Chamber and Main Chamber (layers 13 and 19.3, respectively) indicate the prevalence of hornbeam forest with a mixture of oak and Eurasian linden. This suggests a relatively warm and humid climate, whereas the optical ages place these layers in late MIS 6, during which period generally cold conditions are recorded in Lake Baikal[32,33] (Fig. 4). We caution, however, that climatic conditions may fluctuate greatly within the time resolution of these records (350–1,000 years) and of the optical ages, which have uncertainties of several millennia.

Discussion

The combined Pleistocene sequences from all three chambers provide a near-continuous record of human and environmental history that spans the past three glacial–interglacial cycles (Figs. 3, 4 and Extended Data Table 1). Many layers show signs of post-depositional subsidence, but the deposits have by and large retained their stratigraphic integrity. Disturbance by animal burrowing and other activities is mostly restricted to parts of the uppermost Pleistocene layers, especially close to the cave walls. The timing of the four main artefact phases and the environmental reconstructions are broadly consistent between chambers when taking into account the sampling resolution and the uncertainties associated with palaeoenvironmental records and optical ages.

The oldest stone artefacts and Denisovan fossil indicate that hominins have occupied the cave since late MIS 9 (about 300 ka), with Denisovan DNA retrieved from sediments deposited during late MIS 7, at about 200 ka. The recovery of Denisovan skeletal and genetic remains in younger deposits implies their presence in the cave until early MIS 3 (about 55 ka) and possibly later. Neanderthals were also present from late MIS 7 or early MIS 6 until MIS 5 (about 100 ka), based on fossil and sedimentary DNA evidence. No remains of modern humans have yet been recovered that would confirm their presence at the site during the Late Pleistocene.

The data presented here and in recent genetic studies[12–17,24] reveal that the cave was occupied during the last interglacial by Denisovans and two genetically distinct groups of Neanderthals. Denisovans may have survived until at least about 55 ka, by which time anatomically modern humans were present in other parts of Asia[36–39]. Ongoing investigations at this and other sites in the region may help to resolve the timing and possible causes of extinction of archaic hominins in southern Siberia, and the nature of any encounters—including interbreeding—between them and modern humans.

Online content

Any methods, additional references, Nature Research reporting summaries, source data, statements of data availability and associated accession codes are available at https://doi.org/10.1038/s41586-018-0843-2.

Received: 6 May 2018; Accepted: 30 November 2018;
Published online 30 January 2019.

1. Krause, J. et al. The complete mitochondrial DNA genome of an unknown hominin from southern Siberia. *Nature* **464**, 894–897 (2010).
2. Reich, D. et al. Genetic history of an archaic hominin group from Denisova Cave in Siberia. *Nature* **468**, 1053–1060 (2010).
3. Derevianko, A. P. et al. *Paleoenvironment and Paleolithic Human Occupation of Gorny Altai: Subsistence and Adaptation in the Vicinity of Denisova Cave* (Institute of Archaeology and Ethnography, Siberian Branch of the Russian Academy of Sciences, Novosibirsk, 2003).
4. Bolikhovskaya, N. S. & Shunkov, M. V. Pleistocene environments of northwestern Altai: vegetation and climate. *Archaeol. Ethnol. Anthropol. Eurasia* **42**, 2–17 (2014).
5. Agadjanian, A. K. & Shunkov, M. V. Evolution of the Quaternary environment in the northwestern Altai. *Archaeol. Ethnol. Anthropol. Eurasia* **37**, 2–18 (2009).
6. Bolikhovskaya, N. S., Kozlikin, M. B., Shunkov, M. V., Uliyanov, V. A. & Faustov, S. S. New palynological data from the unique Paleolithic site of Denisova Cave in northwest Altai. *Bull. Moscow Soc. Natural. Biol. Series* **122**, 46–60 (2017).
7. Vasiliev, S. K., Shunkov, M. V. & Kozlikin, M. B. in *Problems of Archaeology, Ethnography and Anthropology of Siberia and Neighbouring Territories* Vol. 23 (eds Derevianko, A. P. et al.) 60–64 (Institute of Archaeology and Ethnography, Siberian Branch of the Russian Academy of Sciences, Novosibirsk, 2017).

8. Turner, C. G. II. in *Chronostratigraphy of the Paleolithic in North Central, East Asia and America* (ed. Derevianko, A. P.) 239–243 (Institute of History, Philology and Philosophy, Siberian Branch of the USSR Academy of Sciences, Novosibirsk, 1990).
9. Shpakova, E. G. & Derevianko, A. P. The interpretation of odontological features of Pleistocene human remains from the Altai. *Archaeol. Ethnol. Anthropol. Eurasia* **1**, 125–138 (2000).
10. Mednikova, M. B. A proximal pedal phalanx of a Paleolithic hominin from Denisova Cave, Altai. *Archaeol. Ethnol. Anthropol. Eurasia* **39**, 129–138 (2011).
11. Meyer, M. et al. A high-coverage genome sequence from an archaic Denisovan individual. *Science* **338**, 222–226 (2012).
12. Sawyer, S. et al. Nuclear and mitochondrial DNA sequences from two Denisovan individuals. *Proc. Natl Acad. Sci. USA* **112**, 15696–15700 (2015).
13. Slon, V. et al. A fourth Denisovan individual. *Sci. Adv.* **3**, e1700186 (2017).
14. Prüfer, K. et al. The complete genome sequence of a Neanderthal from the Altai Mountains. *Nature* **505**, 43–49 (2014).
15. Brown, S. et al. Identification of a new hominin bone from Denisova Cave, Siberia using collagen fingerprinting and mitochondrial DNA analysis. *Sci. Rep.* **6**, 23559 (2016).
16. Slon, V. et al. The genome of the offspring of a Neanderthal mother and a Denisovan father. *Nature* **561**, 113–116 (2018).
17. Slon, V. et al. Neandertal and Denisovan DNA from Pleistocene sediments. *Science* **356**, 605–608 (2017).
18. Vlasov, V. K. & Kulikov, O. A. Radiothermoluminescence dating and applications to Pleistocene sediments. *Phys. Chem. Miner.* **16**, 551–558 (1989).
19. Derevianko, A. P., Laukhin, S. A., Kulikov, O. A., Gnibidenko, Z. N. & Shunkov, M. V. First Middle Pleistocene age determinations of the Paleolithic in the Altai Mountains. *Dokl. Akad. Nauk* **326**, 497–501 (1992).
20. Huntley, D. J. Letters: Vlasov & Kulikov's method. *Anc. TL* **10**, 57–58 (1992).
21. Derevianko, A. P., Gnibidenko, Z. N. & Shunkov, M. V. Middle Pleistocene excursions of the geomagnetic field in the strata of Denisova Cave. *Dokl. Akad. Nauk* **360**, 511–513 (1998).
22. Roberts, A. P. Geomagnetic excursions: knowns and unknowns. *Geophys. Res. Lett.* **35**, L17307 (2008).
23. Laj, C. & Channell, J. E. T. in *Treatise on Geophysics (Volume 5: Geomagnetism)* 2nd edn (ed. Schubert, G.) 343–383 (Elsevier, Amsterdam, 2015).
24. Prüfer, K. et al. A high-coverage Neandertal genome from Vindija Cave in Croatia. *Science* **358**, 655–658 (2017).
25. Huntley, D. J., Godfrey-Smith, D. I. & Thewalt, M. L. W. Optical dating of sediments. *Nature* **313**, 105–107 (1985).
26. Hütt, G., Jaek, I. & Tchonka, J. Optical dating: K-feldspars optical response stimulation spectra. *Quat. Sci. Rev.* **7**, 381–385 (1988).
27. Roberts, R. G. et al. Optical dating in archaeology: thirty years in retrospect and grand challenges for the future. *J. Archaeol. Sci.* **56**, 41–60 (2015).
28. Athanassas, C. D. & Wagner, G. A. Geochronology beyond radiocarbon: optically stimulated luminescence dating of palaeoenvironments and archaeological sites. *Elements* **12**, 27–32 (2016).
29. Shunkov, M. V. et al. The phosphates of Pleistocene–Holocene sediments of the Eastern Gallery of Denisova Cave. *Dokl. Earth Sci.* **478**, 46–50 (2018).
30. Rhodes, E. J. Dating sediments using potassium feldspar single-grain IRSL: initial methodological considerations. *Quat. Int.* **362**, 14–22 (2015).
31. Smedley, R. K., Duller, G. A. T. & Roberts, H. M. Bleaching of the post-IR IRSL signal from individual grains of K-feldspar: implications for single-grain dating. *Radiat. Meas.* **79**, 33–42 (2015).
32. Prokopenko, A. A., Hinnov, L. A., Williams, D. F. & Kuzmin, M. I. Orbital forcing of continental climate during the Pleistocene: a complete astronomically tuned climatic record from Lake Baikal, SE Siberia. *Quat. Sci. Rev.* **25**, 3431–3457 (2006).
33. Grygar, T. et al. Lake Baikal climatic record between 310 and 50 ky BP: interplay between diatoms, watershed weathering and orbital forcing. *Palaeogeogr. Palaeoclimatol. Palaeoecol.* **250**, 50–67 (2007).
34. Melles, M. et al. Sedimentary geochemisty of core PG1351 from Lake El'gygytgyn—a sensitive record of climate variability in the East Siberian Arctic during the past three glacial–interglacial cycles. *J. Paleolimnol.* **37**, 89–104 (2007).
35. Frank, U. et al. A 350 ka record of climate change from Lake El'gygytgyn, Far East Russian Arctic: refining the pattern of climate modes by means of cluster analysis. *Clim. Past* **9**, 1559–1569 (2013).
36. Liu, W. et al. The earliest unequivocally modern humans in southern China. *Nature* **526**, 696–699 (2015).
37. Westaway, K. E. et al. An early modern human presence in Sumatra 73,000–63,000 years ago. *Nature* **548**, 322–325 (2017).
38. Hershkovitz, I. et al. The earliest modern humans outside Africa. *Science* **359**, 456–459 (2018).
39. Groucutt, H. S. et al. *Homo sapiens* in Arabia by 85,000 years ago. *Nat. Ecol. Evol.* **2**, 800–809 (2018).
40. Lisiecki, L. E. & Raymo, M. E. A Pliocene–Pleistocene stack of 57 globally distributed benthic $\delta^{18}O$ records. *Paleoceanography* **20**, PA1003 (2005).

Acknowledgements This study was funded by the Australian Research Council through fellowships to Z.J. (FT150100138), B.L. (FT140100384) and R.G.R. (FL130100116), the Russian Science Foundation (project 14-50-00036 to A.P.D. and A.K.A.), the Russian Foundation for Basic Research (project 17-29-04206 to M.V.S., M.B.K., V.A.U., N.S.B. and S.K.V.) and the state task of the Ministry of Education and Science of the Russian Federation (project 33.867.2017/4.6 to A.P.D.). We thank Y. Jafari, T. Lachlan, D. Müller, D. Tanner, V. Vaneev and the Australian Microscopy & Microanalysis Research Facility for assistance and P. Goldberg for comments on an earlier version of this Article.

Reviewer information *Nature* thanks G. Duller, E. J. Rhodes and the other anonymous reviewer(s) for their contribution to the peer review of this work.

Author contributions Z.J., A.P.D. and R.G.R. conceived this study. M.V.S., M.B.K. and A.P.D. led the excavations and artefact analyses, and Z.J. and B.L. performed the optical dating, with contributions from K.O. and R.G.R. The other analyses were led by V.A.U. (stratigraphy and geoarchaeology), N.S.B. (palynology) and A.K.A. and S.K.V. (palaeontology). Z.J., M.V.S., M.B.K. and R.G.R. wrote the main text with contributions from all authors.

Competing interests The authors declare no competing interests.

Additional information

Extended data is available for this paper at https://doi.org/10.1038/s41586-018-0843-2.
Supplementary information is available for this paper at https://doi.org/10.1038/s41586-018-0843-2.

Correspondence and requests for materials should be addressed to Z.J. or R.G.R.

METHODS

No statistical methods were used to predetermine sample size. The experiments were not randomized and investigators were not blinded to allocation during experiments and outcome assessment.

Sediment samples for optical dating were collected at Denisova Cave in 2012, 2014, 2016 and 2017. Samples were collected by hand at night using a red-light torch for illumination, and sealed in thick black plastic to prevent light exposure during transport to the University of Wollongong. Optical dating gives an estimate of the time since grains of minerals, such as quartz and K-feldspar, were last exposed to sunlight[25–28]. The time of sediment deposition is estimated by dividing the equivalent dose (D_e, the radiation energy absorbed by grains since deposition) by the environmental dose rate (the rate of supply of oinizing radiation to the grains since deposition). The D_e is estimated from laboratory measurements of the OSL from quartz or the pIRIR from K-feldspar. The OSL signal is bleached by light more rapidly and completely than the pIRIR signal[30,31] (hence, consistent OSL and pIRIR ages suggests prolonged bleaching at deposition) but the latter signal saturates at much higher doses than the OSL signal[27,28] (hence, finite ages can be obtained for older deposits). The dose rate is estimated from field and laboratory measurements of environmental radioactivity, plus the small contribution from cosmic rays.

We used both quartz and K-feldspar grains to develop a numerical chronology for the Pleistocene sequences in Denisova Cave. The ages of the older samples were determined solely from the K-feldspar pIRIR signal, owing to saturation of the quartz OSL signal. Standard procedures were used to isolate individual grains of quartz (180–212 μm in diameter) and K-feldspar (ranging in size between 90 and 212 μm in diameter, depending on availability), and grains were etched in hydrofluoric acid to remove the alpha-irradiated surface layer. D_e values for individual quartz grains were estimated using well-established OSL measurement and data-analysis procedures[41–43], and D_e values for individual K-feldspar grains were determined using a two-step (200 °C and 275 °C) regenerative-dose pIRIR procedure[44] and a recently developed standardized growth curve approach[45,46]. We analysed the single-grain pIRIR signals in two ways to estimate the final D_e values. A multiple-aliquot regenerative-dose procedure for K-feldspar was used to estimate the D_e values for the oldest deposits[47]. Details of sample preparation and D_e determination methods, experimental procedures, quality-assurance criteria and validation tests are given in the Supplementary Information.

The environmental dose rate includes contributions from beta particles (measured in the laboratory[48] on a portion of each sample), gamma rays (measured by in situ gamma spectrometry at each sample location), cosmic rays[49] and radioactive emitters internal to the K-feldspar and quartz grains. The latter dose rate is commonly trivial for quartz (we assumed a value of 0.032 ± 0.010 Gy per thousand years), but is substantial for K-feldspar owing to the beta dose from ^{40}K; we measured the potassium contents of a subset of grains by wavelength-dispersive X-ray spectroscopy using an electron microprobe. The measured beta dose rates were corrected for grain-size attenuation, and the beta, gamma and cosmic-ray dose rates were adjusted for water content (based on the measured field values). The sample D_e values were divided by the corresponding total environmental dose rates to calculate the optical ages in calendar years before present; the associated uncertainties are at the 68.2% confidence level and include all known and estimated sources of random and systematic error. Details of dose-rate determination and the resulting data are presented in the Supplementary Information, together with the age determination and error estimation procedures.

A Bayesian age model was developed separately for Main Chamber, East Chamber and South Chamber on the OxCal platform[50,51]. Each age was input as a C_date in calendar years before AD 1950 with an associated uncertainty (the standard error of the mean); we used the weighted mean age for each of the samples with paired OSL and pIRIR ages. The sequence of stratigraphic layers in each chamber was used as prior information, and we also allowed for the probable existence of time gaps (modelled as intervals) in each stratigraphic sequence; the resulting ages, however, are insensitive to the choice of model. Each sequence was modelled as a series of phases, assuming that (a) the stratigraphically lowest phase is older than those above, and (b) the measured ages are unordered and uniformly distributed within each phase. Modelled age estimates were obtained for the start and end of each phase to facilitate chronological comparisons between the three chambers. Details of the Bayesian modelling and the resulting chronologies are provided in the Supplementary Information.

Code availability. All custom R code used to produce the results presented here are available from the corresponding authors on reasonable request.

Reporting summary. Further information on research design is available in the Nature Research Reporting Summary linked to this paper.

Data availability

All data generated and/or analysed during the current study are available from the corresponding authors on reasonable request.

41. Jacobs, Z. & Roberts, R. G. Advances in optically stimulated luminescence dating of individual grains of quartz from archeological deposits. *Evol. Anthropol.* **16**, 210–223 (2007).
42. Wood, R. et al. Towards an accurate and precise chronology for the colonization of Australia: the example of Riwi, Kimberley, Western Australia. *PLoS ONE* **11**, e0160123 (2016).
43. Clarkson, C. et al. Human occupation of northern Australia by 65,000 years ago. *Nature* **547**, 306–310 (2017).
44. Blegen, N. et al. Distal tephras of the eastern Lake Victoria basin, equatorial East Africa: correlations, chronology and a context for early modern humans. *Quat. Sci. Rev.* **122**, 89–111 (2015).
45. Li, B., Jacobs, Z., Roberts, R. G., Galbraith, R. & Peng, J. Variability in quartz OSL signals caused by measurement uncertainties: problems and solutions. *Quat. Geochronol.* **41**, 11–25 (2017).
46. Li, B., Jacobs, Z., Roberts, R. G. & Li, S.-H. Single-grain dating of potassium-rich feldspar grains: towards a global standardised growth curve for the post-IR IRSL signal. *Quat. Geochronol.* **45**, 23–36 (2018).
47. Li, B., Jacobs, Z. & Roberts, R. G. An improved multiple-aliquot regenerative-dose (MAR) procedure for post-IR IRSL dating of K-feldspar. *Anc. TL* **35**, 1–10 (2017).
48. Bøtter-Jensen, L. & Mejdahl, V. Assessment of beta dose-rate using a GM multicounter system. *Nucl. Tracks Radiat. Meas.* **14**, 187–191 (1988).
49. Prescott, J. R. & Hutton, J. T. Cosmic ray contributions to dose rates for luminescence and ESR dating: large depths and long-term time variations. *Radiat. Meas.* **23**, 497–500 (1994).
50. Bronk Ramsey, C. Bayesian analysis of radiocarbon dates. *Radiocarbon* **51**, 337–360 (2009).
51. Bronk Ramsey, C. & Lee, S. Recent and planned developments of the program OxCal. *Radiocarbon* **55**, 720–730 (2013).

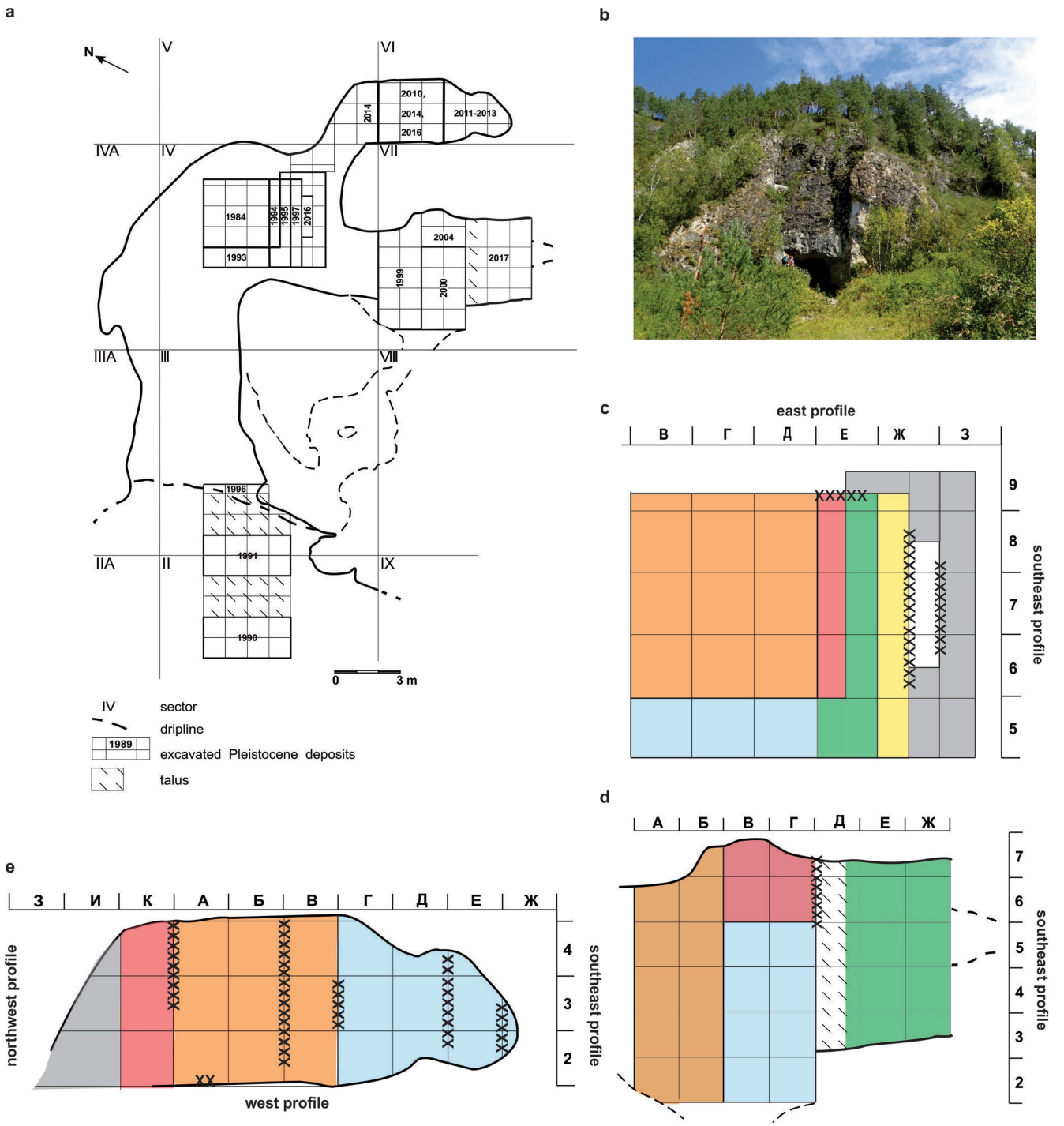

Extended Data Fig. 1 | Plan maps of Main Chamber, East Chamber and South Chamber in Denisova Cave. a, Detailed plan of cave interior, showing year of excavation in each of the chambers and at the cave entrance. **b**, Photograph of the present-day cave entrance, with people on the left for scale. **c**–**e**, Plan maps of Main Chamber (**c**), South Chamber (**d**) and East Chamber (**e**), with the sequence of excavations in each chamber denoted by colour shading: from orange (earliest) through blue, pink, green and yellow, to white (most recent), with unexcavated areas in grey. Crosses denote locations of optical dating samples in each profile.

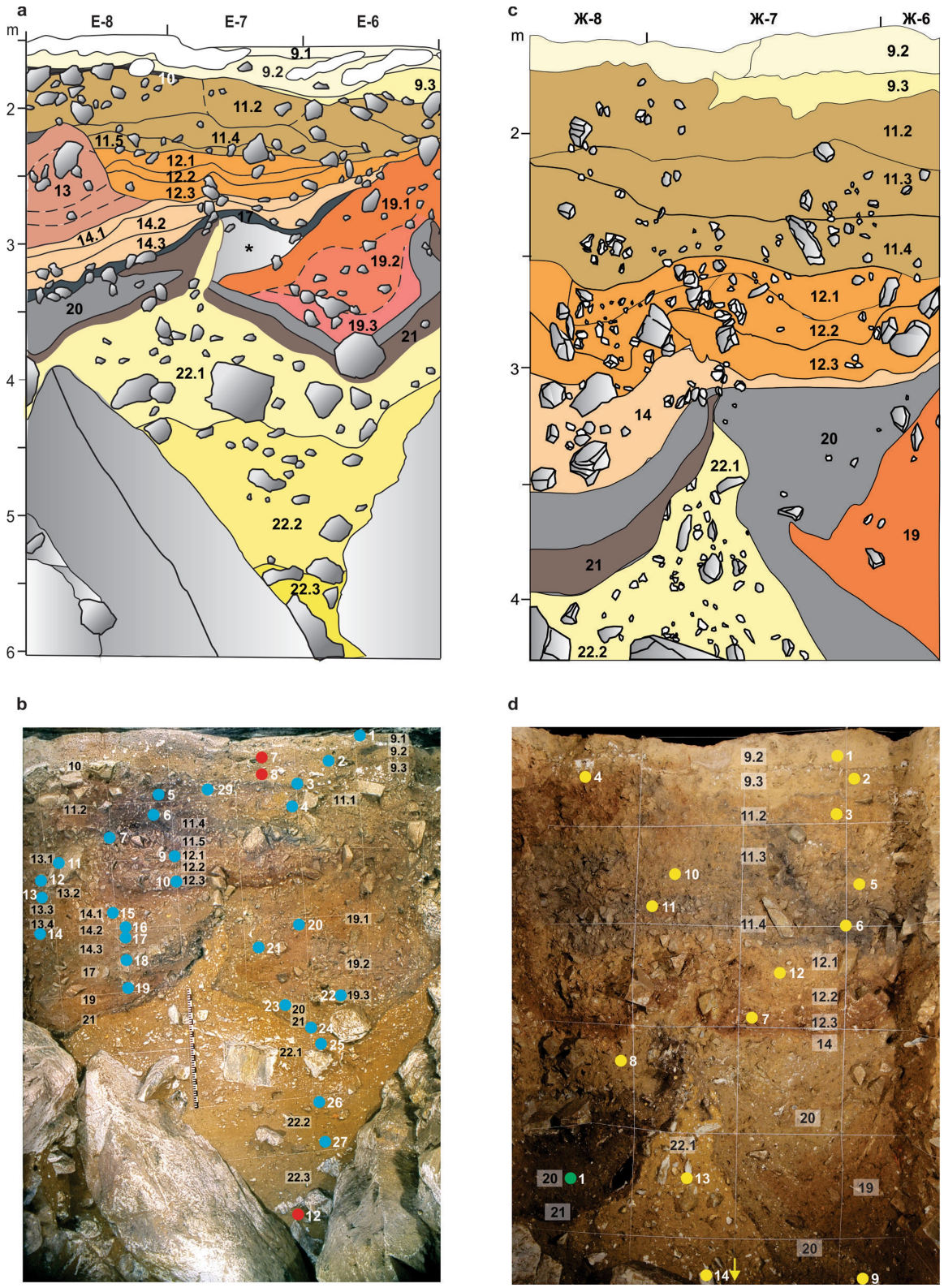

Extended Data Fig. 2 | Stratigraphic sequences and locations of optical dating samples in Main Chamber. a, **b**, Southeast profile after excavations in 1984 (**a**) and locations of samples collected from this profile in 2012 (blue) and 2014 (red) (**b**). **c**, **d**, Southeast profile after excavations in 2016 (**c**) and locations of samples collected from this profile in 2016 (yellow) (**d**). The number next to each filled circle represents the sample code (for example, number 1 next to the blue-filled circle in **b** denotes sample DCM12-1).

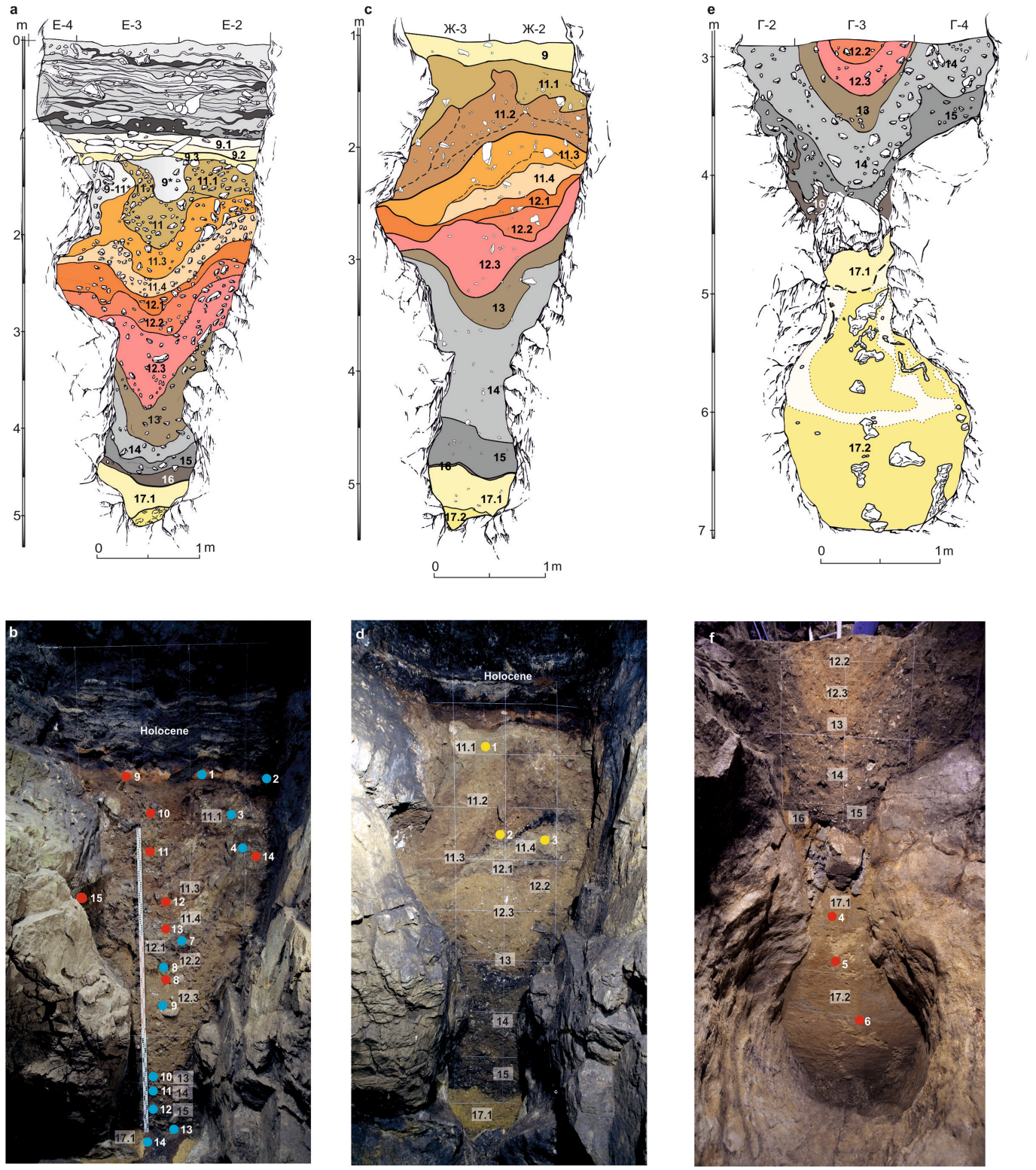

Extended Data Fig. 3 | Stratigraphic sequences and locations of optical dating samples in East Chamber. a, **b**, Southeast profile after excavations in 2012 (**a**) and locations of samples collected from this profile in 2012 (blue) and 2014 (red) (**b**). **c**, **d**, Southeast profile after excavations in 2015 (**c**) and locations of samples collected from this profile in 2016 (yellow) (**d**). **e**, **f**, Lower section of northwest profile (that is, below the choke-stone blocking the gap between the middle and lower sections of the hourglass-shaped cave profile) after excavations in 2014 (**e**) and locations of samples collected from this profile in 2014 (**f**). The number next to each filled circle represents the sample code (for example, number 1 next to the blue-filled circle in **b** denotes sample DCE12-1).

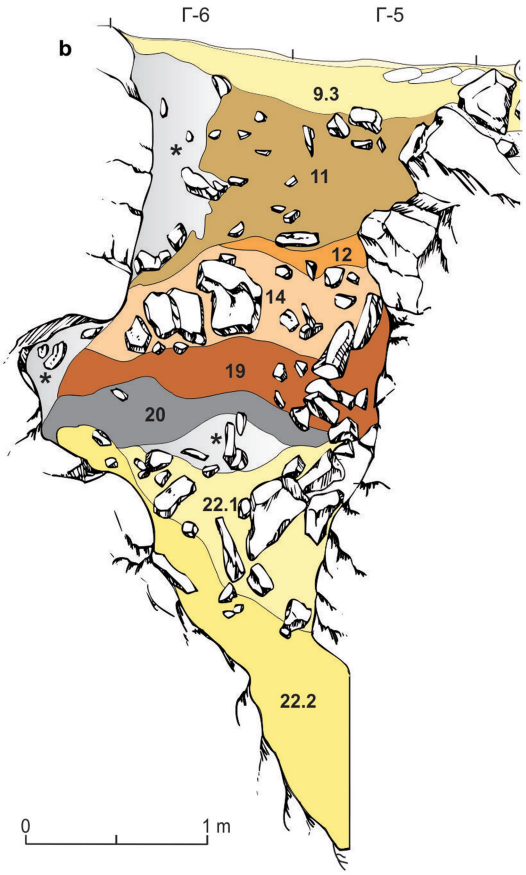

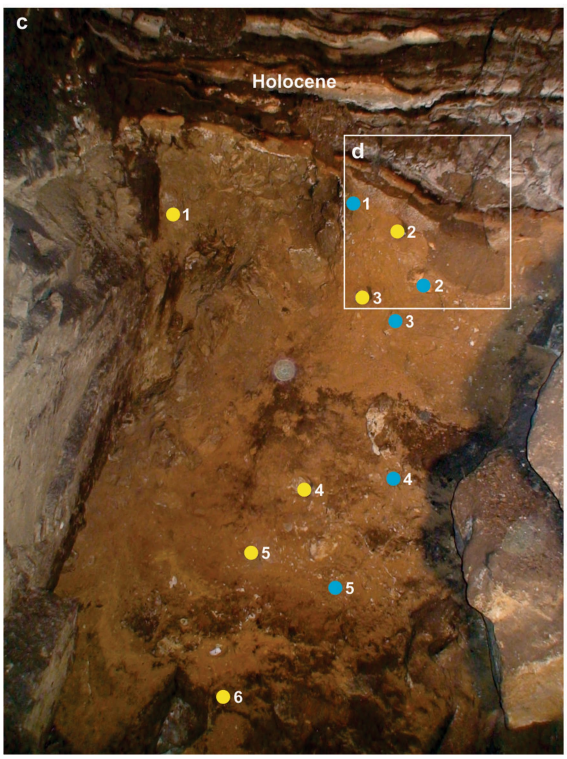

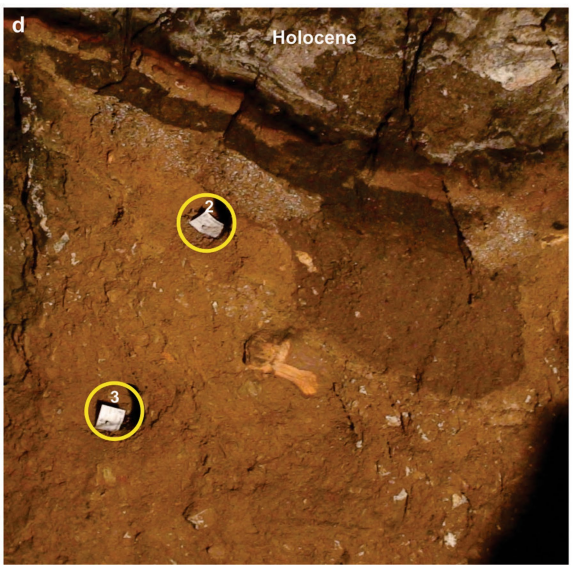

Extended Data Fig. 4 | Stratigraphic sequences and locations of optical dating samples in South Chamber. a–**c**, Southeast profile after excavations in 2003 (**a**, **b**) and after excavations in 2016 (**c**), showing locations of samples collected in 2012 (blue) and 2016 (yellow). The number next to each filled circle represents the sample code (for example, number 1 next to the blue-filled circle denotes sample DCS12-1). **d**, Area enclosed by the white square in **c**. Sample DCS16-2 is located about 13 cm below the base of the Holocene deposits and to the left of an infilled animal burrow, and immediately beneath a zone of phosphatization.

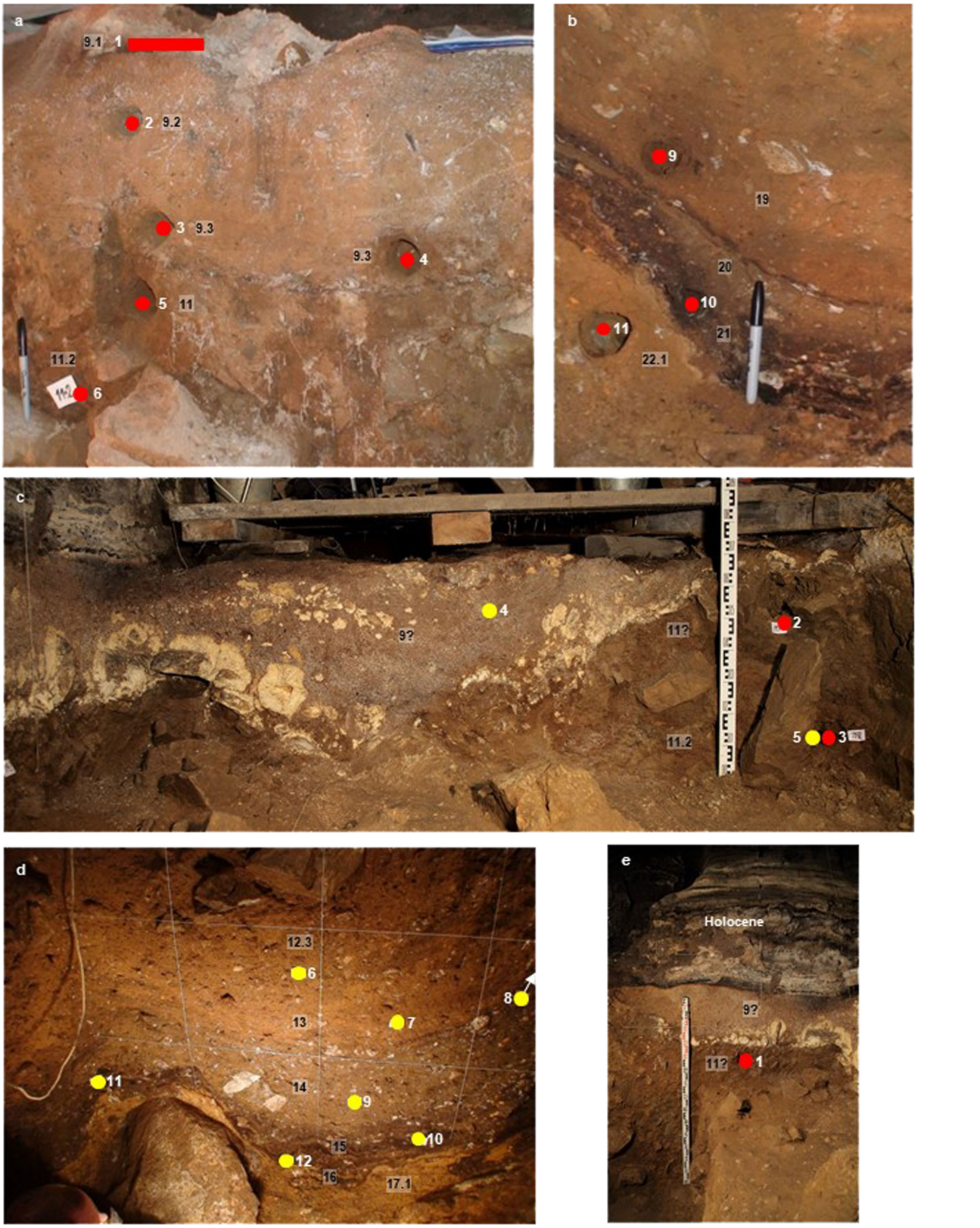

Extended Data Fig. 5 | Additional stratigraphic sequences and sampling locations in Main Chamber and East Chamber. a, Upper section of east profile in Main Chamber, showing locations of optical dating samples collected in 2014. **b**, Lower section of east profile in Main Chamber, showing locations of samples collected in 2014. **c**, Upper section of northwest profile in East Chamber, showing locations of samples collected in 2014 (red) and 2016 (yellow). **d**, Middle section of northwest profile in East Chamber, showing locations of samples collected in 2016. The lower section of this profile is shown in Extended Data Fig. 3f. **e**, West profile in East Chamber, showing location of sample DCE14-1.

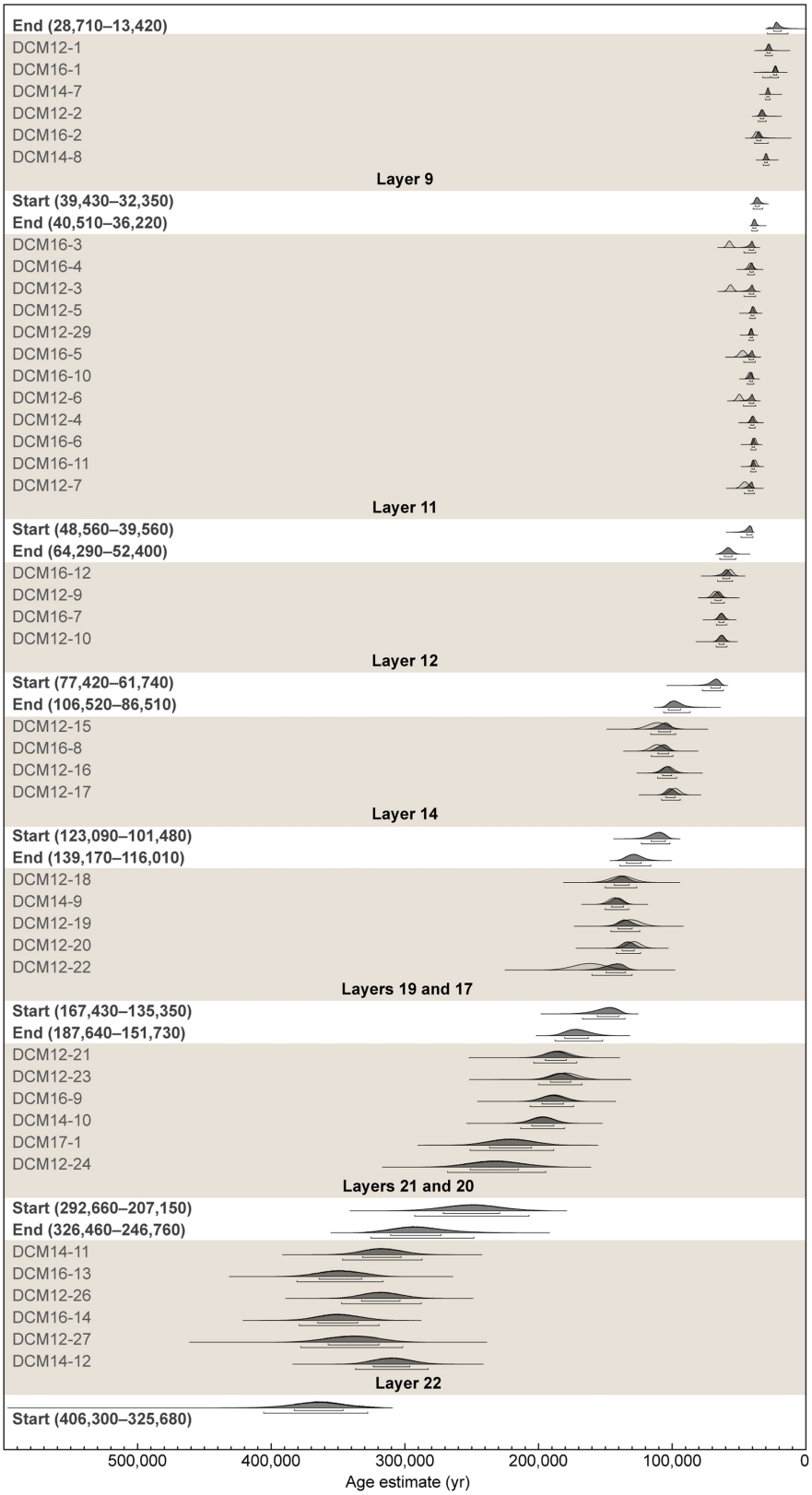

Extended Data Fig. 6 | Bayesian model of optical ages for deposits in Main Chamber. Ages ($n = 43$) have been modelled in OxCal version 4.2.4. Only random errors are included in the age model. Pale probability distributions represent the unmodelled ages (likelihoods) and dark grey distributions represent the modelled ages (posterior probabilities). The narrow and wide brackets beneath the distributions represent the 68.2% and 95.4% probability ranges, respectively. Start and end ages have been modelled for each phase, with age ranges (95.4% confidence interval, random-only errors) given in years and rounded off to the closest decade.

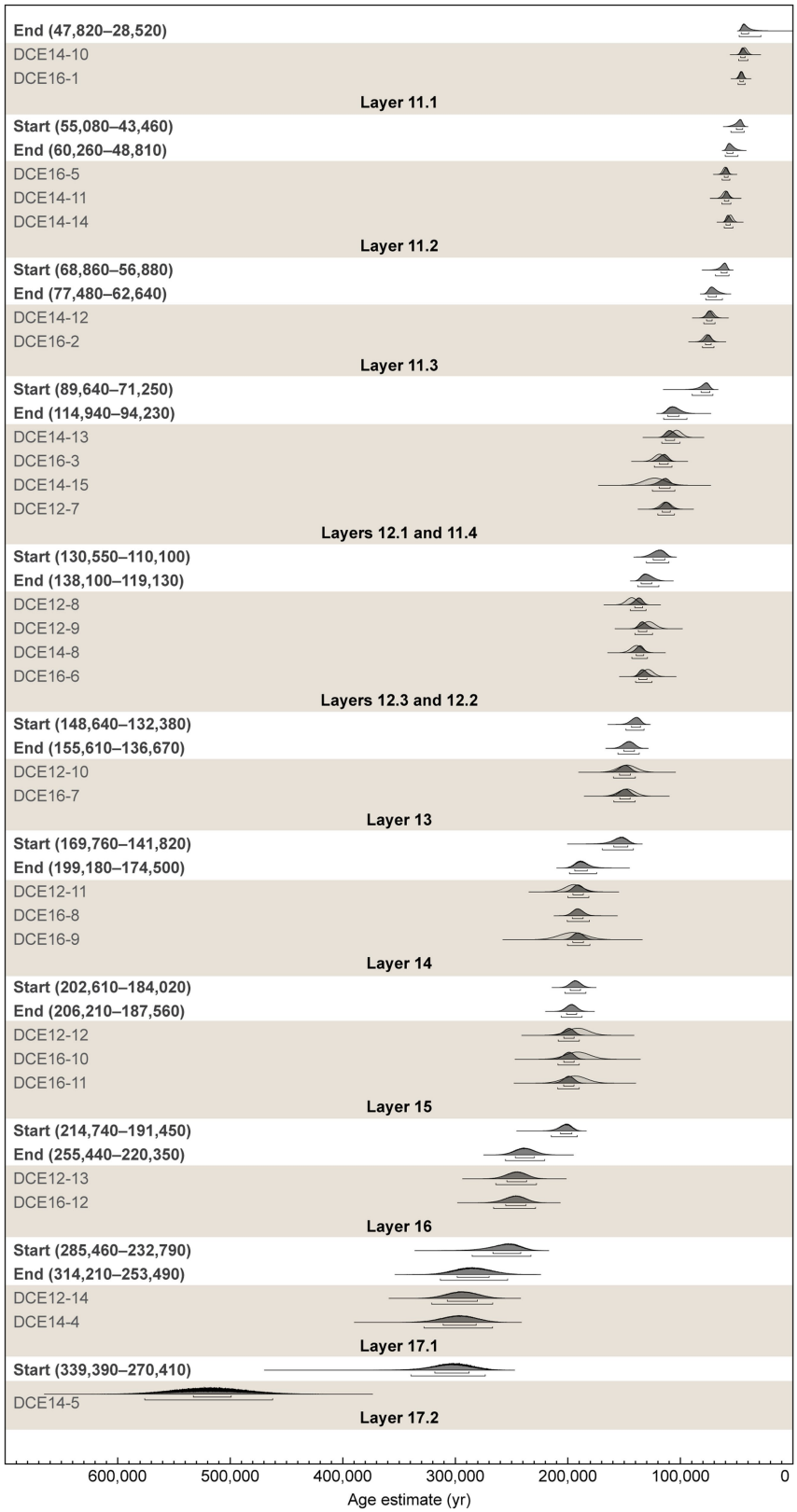

Extended Data Fig. 7 | Bayesian model of optical ages for deposits in East Chamber. Ages ($n = 28$) have been modelled in OxCal version 4.2.4. Only random errors are included in the age model. Pale probability distributions represent the unmodelled ages (likelihoods) and dark grey distributions represent the modelled ages (posterior probabilities). The narrow and wide brackets beneath the distributions represent the 68.2% and 95.4% probability ranges, respectively. Start and end ages have been modelled for each phase, with age ranges (95.4% confidence interval, random-only errors) given in years and rounded off to the closest decade.

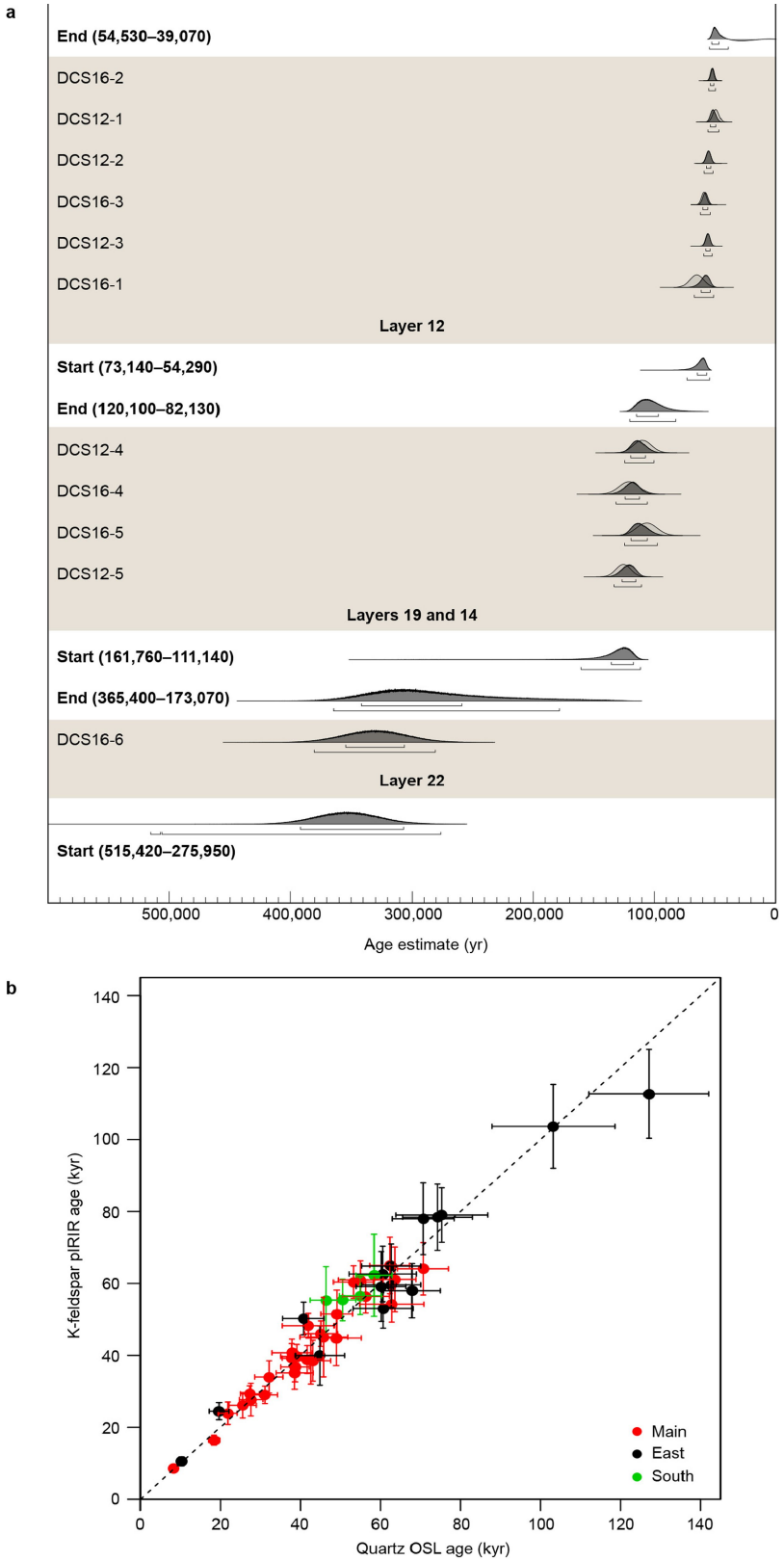

Extended Data Fig. 8 | Bayesian model of optical ages for deposits in South Chamber and comparison of OSL and pIRIR ages for all three chambers. a, Ages ($n = 11$) have been modelled in OxCal version 4.2.4. Only random errors are included in the age model. Pale probability distributions represent the unmodelled ages (likelihoods) and dark grey distributions represent the modelled ages (posterior probabilities). The narrow and wide brackets beneath the distributions represent the 68.2% and 95.4% probability ranges, respectively. Start and end ages have been modelled for each phase, with age ranges (95.4% confidence interval, random-only errors) given in years and rounded off to the closest decade. **b**, Comparison of single-grain OSL ages for quartz and single-grain pIRIR ages for K-feldspar for 47 samples (28 from Main Chamber, 15 from East Chamber and 4 from South Chamber), with age uncertainties shown at 2σ. The dashed line indicates the 1:1 ratio.

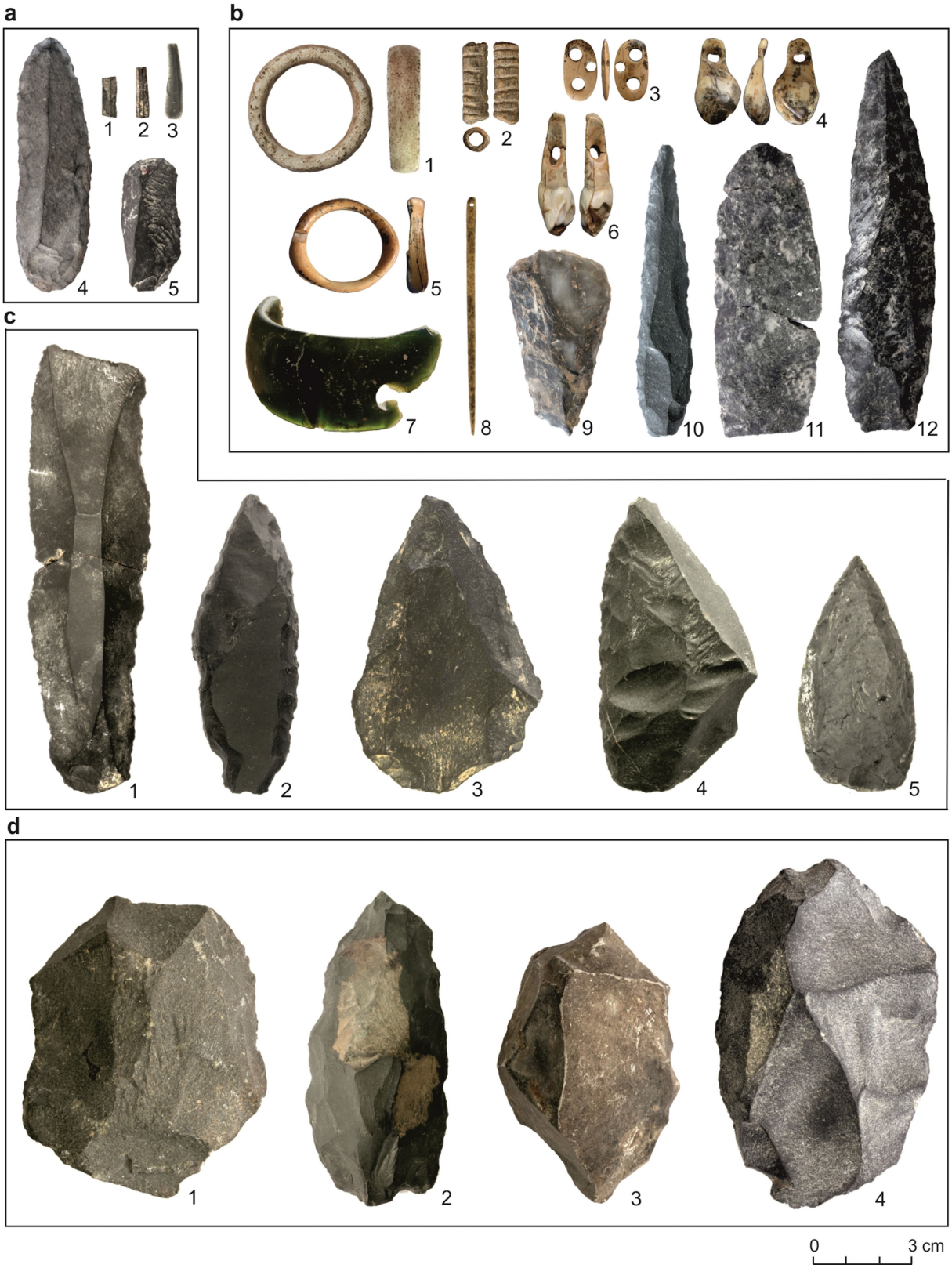

Extended Data Fig. 9 | Palaeolithic artefacts from Main Chamber, East Chamber and South Chamber. a, Upper Palaeolithic artefacts. 1–3, bladelets; 4, retouched blade; and 5, end-scraper. **b**, Initial Upper Palaeolithic artefacts. 1, marble ring; 2, tubular beads; 3, ivory pendant; 4, pendant made of red deer tooth; 5, ivory ring; 6, pendant made of elk tooth; 7, chloritolite bracelet; 8, bone needle; 9, end-scraper; 10, retouched point; 11, biface; and 12, pointed blade. **c**, Artefacts of middle Middle Palaeolithic assemblage. 1, blade; 2 and 5, Mousterian points; 3, Levallois point; and 4, scraper. **d**, Early Middle Palaeolithic assemblage. 1, core; 2 and 4, scrapers; 3, denticulate tool.

Extended Data Table 1 | Compilation of modelled start and end ages for Main Chamber, East Chamber and South Chamber

Archaeology	Main Chamber			East Chamber			South Chamber		
	Layer	Age ± 2σ (kyr)		Layer	Age ± 2 σ (kyr)		Layer	Age ± 2 σ (kyr)	
Upper Palaeolithic	9	end	21 ± 8	9			9		
		start	36 ± 4						
Initial Upper Palaeolithic	11	end	38 ± 3	11.1	end	38 ± 9	11		
		start	44 ± 5		start	49 ± 6		end	47 ± 8
		gap	13 ± 5	11.2	end	55 ± 6	12		
middle Middle Palaeolithic	12	end	58 ± 6		start	63 ± 6			
		start	70 ± 8	11.3	end	70 ± 8		start	64 ± 9
		gap	26 ± 10		start	80 ± 10		gap	39 ± 21
					gap	25 ± 13			
	14	end	97 ± 11	11.4	end	105 ± 11	14	end	101 ± 19
		start	112 ± 12						
		gap	13 ± 10	12.1	start	120 ± 11			
	17	end	128 ± 13	12.2	end	129 ± 11			
				12.3	start	141 ± 10	19	start	136 ± 26
				13	end	146 ± 11			
	19	start	151 ± 17		start	156 ± 15			
		gap	16 ± 13		gap	32 ± 18			
early Middle Palaeolithic	20	end	170 ± 19	14	end	187 ± 14			
					start	193 ± 12		gap	135 ± 106
				15	end	197 ± 12			
					start	203 ± 14			
					gap	36 ± 17			
				16	end	238 ± 20			
	21	start	250 ± 44		start	259 ± 28			
		gap	29 ± 26				22	end	269 ± 97
	22.1	end	287 ± 41	17.1	end	284 ± 32			
					start	305 ± 37			
sterile	22.3	start	366 ± 43		gap	214 ± 74	22	start	396 ± 121
				17.2		508 ± 40			

Modelled mean ages obtained from the Bayesian model results presented in Extended Data Figs. 6–8 and their estimated uncertainties ($\pm 2\sigma$) are presented for each layer (or combination of layers) together with their archaeological associations, which have been colour-coded to differentiate the four main artefact phases (early Middle Palaeolithic, dark green; middle Middle Palaeolithic, pale green; Initial Upper Palaeolithic, dark orange; and Upper Palaeolithic, pale orange). Modelled time intervals, representing potential gaps in the stratigraphic sequences, are shaded grey, with their estimated durations ($\pm 2\sigma$) given in thousands of years.

nature research

Corresponding author(s): Zenobia Jacobs, Richard G. Roberts

Reporting Summary

Nature Research wishes to improve the reproducibility of the work that we publish. This form provides structure for consistency and transparency in reporting. For further information on Nature Research policies, see Authors & Referees and the Editorial Policy Checklist.

Statistical parameters

When statistical analyses are reported, confirm that the following items are present in the relevant location (e.g. figure legend, table legend, main text, or Methods section).

n/a	Confirmed	
☐	☒	The exact sample size (*n*) for each experimental group/condition, given as a discrete number and unit of measurement
☐	☒	An indication of whether measurements were taken from distinct samples or whether the same sample was measured repeatedly
☒	☐	The statistical test(s) used AND whether they are one- or two-sided *Only common tests should be described solely by name; describe more complex techniques in the Methods section.*
☒	☐	A description of all covariates tested
☒	☐	A description of any assumptions or corrections, such as tests of normality and adjustment for multiple comparisons
☐	☒	A full description of the statistics including central tendency (e.g. means) or other basic estimates (e.g. regression coefficient) AND variation (e.g. standard deviation) or associated estimates of uncertainty (e.g. confidence intervals)
☒	☐	For null hypothesis testing, the test statistic (e.g. *F*, *t*, *r*) with confidence intervals, effect sizes, degrees of freedom and *P* value noted *Give P values as exact values whenever suitable.*
☐	☒	For Bayesian analysis, information on the choice of priors and Markov chain Monte Carlo settings
☒	☐	For hierarchical and complex designs, identification of the appropriate level for tests and full reporting of outcomes
☒	☐	Estimates of effect sizes (e.g. Cohen's *d*, Pearson's *r*), indicating how they were calculated
☐	☒	Clearly defined error bars *State explicitly what error bars represent (e.g. SD, SE, CI)*

Our web collection on statistics for biologists may be useful.

Software and code

Policy information about availability of computer code

Data collection	For collection of the luminescence data, software specific to the instruments (Riso TL-DA-20) was used.
Data analysis	For analysis of the luminescence data, the R-packages 'numOSL' and 'Luminescence' were used for curve fitting, equivalent-dose estimation, error estimation, age model analysis and graphical display. Details of this open-source package and functions used are provided in Peng et al. (2013), Peng & Li (2017) and Kreutzer et al (2012), all of which are referenced in Supplementary Information (refs 78 and 79). For Bayesian age modelling, the OxCal 4.2.4 platform was used. The CQL codes used to generate the age models for the Main, East and South Chambers of Denisova Cave are given in Supplementary Tables 13, 14 and 15, respectively.

For manuscripts utilizing custom algorithms or software that are central to the research but not yet described in published literature, software must be made available to editors/reviewers upon request. We strongly encourage code deposition in a community repository (e.g. GitHub). See the Nature Research guidelines for submitting code & software for further information.

Data

Policy information about availability of data

All manuscripts must include a data availability statement. This statement should provide the following information, where applicable:

- Accession codes, unique identifiers, or web links for publicly available datasets
- A list of figures that have associated raw data
- A description of any restrictions on data availability

The luminescence datasets generated in this study are presented in Extended Data Figs 6-8, Extended Data Table 1, Supplementary Tables 4-12 and Supplementary Figs 1-16. All other relevant data are available from the corresponding authors on request.

Field-specific reporting

Please select the best fit for your research. If you are not sure, read the appropriate sections before making your selection.

☐ Life sciences ☐ Behavioural & social sciences ☒ Ecological, evolutionary & environmental sciences

For a reference copy of the document with all sections, see nature.com/authors/policies/ReportingSummary-flat.pdf

Ecological, evolutionary & environmental sciences study design

All studies must disclose on these points even when the disclosure is negative.

Study description	Sediment samples were collected for optical dating from a cave site in southern Siberia (Denisova Cave)
Research sample	A total of 103 sediment samples were collected for OSL dating from vertical profiles exposed during excavation of the cave deposits. Samples were collected from stratigraphic layers at suitable locations in 2012, 2014, 2016 and 2017. Artefacts, hominin (Denisovan and Neanderthal) fossils, and the remains of the fauna and flora have been collected previously, with all relevant references cited in the paper.
Sampling strategy	Our aim was to collect and date samples from as many of the Pleistocene sedimentary layers as possible to obtain a detailed horizontal and vertical coverage of the sediments from the site. Samples were continuously collected during four excavation seasons in 2012, 2014, 2016 and 2017 from both old and freshly excavated profiles. The sample size was determined based on dating results obtained from each year since 2012. For a particular stratigraphic layer, if dating results in one year provided interesting insights about the formation of the site or deposition of the sediments, then further samples were collected in the subsequent year to verify the results. It was also paramount to obtain at least one reliable repeat samples from each layer to check for reproducibility.
Data collection	Samples were collected for optical dating primarily by Z.J. and R.G.R with help from B.L and K.O. by removing sediment from profiles using a metal corer under red light at night time. A sub-sample was also collected for measurement of the radioactivity of the sediment. Samples for luminescence data were measured by Z.J. and B.L. using Risø TL/OSL readers and analysed by Z.J. and B.L. using a range of different customised software. Samples for measurement of the radioactivity of each samples was conducted by Z.J. and R.G.R in the field using a field gamma spectrometer and in the laboratory using a GM-25-5 beta counter. A check on the beta dose rates were also obtained by an independent laboratory through measurements of potassium, uranium and thorium using inductively-coupled plasma mass spectrometry. Data for sediments and stratigraphy, artefacts, hominin (Denisovan and Neanderthal) fossils, and the remains of the fauna and flora have been collected by our Russian co-authors.
Timing and spatial scale	The project was initiated in 2011 when a memorandum of understanding was signed between the University of Wollongong and the Russian Academy of Sciences, Siberian Branch. Our first sampling trip under this MOU commenced in 2012. It initially took some time to ship samples from Russia to Australia (~9-12 months from sampling) and we needed time to develop appropriate measurement procedures for the samples. A sampling field trip for collection of additional samples to fill gaps and to target freshly excavated areas then took place in alternate years. So, the whole project was necessarily protracted. The sampling frequency was strategically planned based on the progress of archaeological excavation at Denisova Cave, and the ongoing dating work in the laboratory. Artefacts, hominin fossils, and the remains of the fauna and flora have been collected at various times over the last 40 years.
Data exclusions	All data collected were analysed and contributed to the final conclusions.
Reproducibility	This study involved measurements of multiple, individual quartz and K-feldspar grains, yielding distributions of equivalent-dose estimates from which the weighted mean was calculated using well-established statistical models (refs 73, 92 and 101 in Supplementary Information). For a few samples, multiple-aliquot measurements were required to estimate the equivalent dose. The distributions of equivalent-dose values for all samples are shown in Supplementary Figs 1-18, together with additional supporting luminescence data. Reproducibility of the beta dose rates was also assessed directly using independent methods, as described in Supplementary Information and presented in Supplementary Fig. 15. A comparison of quartz and K-feldspar ages for the 47 relevant samples are displayed in Extended Data Fig. 8b. All attempts at replication were successful.
Randomization	No randomization was done. Samples were collected from stratigraphic layers exposed during excavations in 2012, 2014, 2016 and 2017.

Blinding	No blinding was done, either for sample collection or analysis. Samples were collected and processed using the procedures described in Methods and Supplementary Information.

Did the study involve field work? ☒ Yes ☐ No

Field work, collection and transport

Field conditions	Samples were collected in August 2012, 2014, 2016 and 2017 from inside Denisova Cave, where conditions were cool and dry.
Location	Denisova Cave is located at 51°23'51.3" N, 84°40'34.3"E and elevated 670 m above sea level.
Access and import/export	Sediment samples were exported from Russia to Australia under appropriate Russian permits: For samples collected in August 2012 Name of issuing authority: the Novosibirsk Customs Office Date of issue: 27/08/2013 Identifying information: a stamp from the Novosibirsk Customs Office on the customs declaration, saying "Approved For Released" and showing a release date. It goes without a particular number. For samples collected in August 2014 Name of issuing authority: the Novosibirsk Customs Office Date of issue: 14/05/2015 Identifying information: a stamp from the Novosibirsk Customs Office on the customs declaration, saying "Approved For Released" and showing a release date. It goes without a particular number. For samples collected in August 2016 Name of issuing authority: the Novosibirsk Customs Office Date of issue: 18/04/2017 Identifying information: a stamp from the Novosibirsk Customs Office on the customs declaration, saying "Approved For Released" and showing a release date. It goes without a particular number. For samples collected in August 2017 Name of issuing authority: the Novosibirsk Customs Office Date of issue: 16/04/2018 Identifying information: a stamp from the Novosibirsk Customs Office on the customs declaration, saying "Approved For Released" and showing a release date. It goes without a particular number. All samples are imported into Australia under an appropriate permit for quarantined materials awarded to Richard Roberts at the University of Wollongong. For samples collected in August 2012 Name of issuing authority: Australian Government, Department of Agriculture, Fisheries and Forestry Date of issue: 01/03/2012 valid till 01/03/2014 Identifying information: Permit number IP12003422 For samples collected in August 2014 Name of issuing authority: Australian Government, Department of Agriculture, Fisheries and Forestry Date of issue: 24/03/2014 valid till 24/03/2016 Identifying information: Permit number IP14002361 For samples collected in August 2016 and August 2017 Name of issuing authority: Australian Government, Department of Agriculture and Water Resources Date of issue: 21/06/2016 valid till 21/06/2018 Identifying information: Permit number 0000480685
Disturbance	This site has been excavating continuously by archaeologists. We took OSL samples for dating from exposed profiles after each excavation season under the supervision of archaeologists so that disturbance was minimised. The site was closed and protected at the end of each excavation season and there is a full-time caretaker that lives near the site.

Reporting for specific materials, systems and methods

Materials & experimental systems

n/a	Involved in the study
☒	☐ Unique biological materials
☒	☐ Antibodies
☒	☐ Eukaryotic cell lines
☒	☐ Palaeontology
☒	☐ Animals and other organisms
☒	☐ Human research participants

Methods

n/a	Involved in the study
☒	☐ ChIP-seq
☒	☐ Flow cytometry
☒	☐ MRI-based neuroimaging